NANO LETTERS

Letter

pubs.acs.org/NanoLett

Plasmonic Color Filters for CMOS Image Sensor Applications

Sozo Yokogawa,[†,‡,§] Stanley P. Burgos,[†,§] and Harry A. Atwater*[,†]

[†]Thomas J. Watson Laboratories of Applied Physics, California Institute of Technology, Pasadena, California 91125, United States

[‡]Sony Corporation, Atsugi Tec. 4-14-1 Asahi-cho, Atsugi, Kanagawa, 243-0014, Japan

ABSTRACT: We report on the optical properties of plasmonic hole arrays as they apply to requirements for plasmonic color filters designed for state-of-the-art Si CMOS image sensors. The hole arrays are composed of hexagonally packed subwavelength sized holes on a 150 nm Al film designed to operate at the primary colors of red, green, and blue. Hole array plasmonic filters show peak transmission in the 40−50% range for large (>5 × 5 μm^2) size filters and maintain their filtering function for pixel sizes as small as ∼1 × 1 μm^2, albeit at a cost in transmission efficiency. Hole array filters are found to robust with respect to spatial crosstalk between pixel within our detection limit and preserve their filtering function in arrays containing random defects. Analysis of hole array filter transmittance and crosstalk suggests that nearest neighbor hole−hole interactions rather than long-range interactions play the dominant role in the transmission properties of plasmonic hole array filters. We verify this via a simple nearest neighbor model that correctly predicts the hole array transmission efficiency as a function of the number of holes.

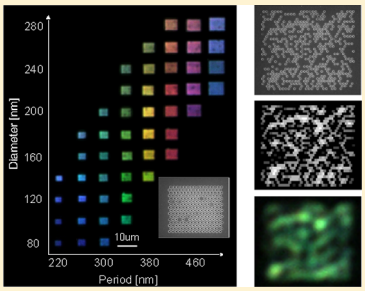

KEYWORDS: *Plasmonics, hole array filter, CMOS image sensor*

Metal films with subwavelength-size periodic hole arrays are known to act as optical filters owing to the interference of surface plasmon polaritons (SPPs) between adjacent holes. Unlike current on-chip organic color filters, plasmonic filters have the advantage of high color-tunability with only a single perforated metal layer and do not suffer from performance degradation after ultraviolet (UV) radiation. However, for successful on-chip implementation, the plasmonic filter must also be compatible with contemporary image sensors featuring small (∼1 × 1 μm^2) pixel size, and large functional array size, spatial color-crosstalk effects, and robustness against random defects.

Extensive studies of enhanced transmission through optically thick metal films perforated with arrays of subwavelength size holes have been performed by numerous groups.[1−7] The enhanced transmission observed in hole arrays is explained by excitation of surface plasmon polaritons (SPPs) at the metal surface that are launched at each hole and interfered among adjacent holes. Transmission enhancements are found to occur at central frequencies determined by the physical size of the holes and thickness of metal film, as well as the optical properties of metal and dielectric medium.[5,6] With reported peak transmission efficiencies of more than 30% at visible wavelengths, hole array films have received much attention for their potential to serve as spectral filters for imaging applications.[8−10]

In contemporary image sensor technologies such as CCDs and CMOS image sensors (CISs), color sensitivity is added to photodetective pixels by equipping them with on-chip color filters (OCCFs), typically composed of organic dyes corresponding to the three primary colors. However, organic dye filters are not being durable at high temperatures or under long-duration ultraviolet irradiation exposure and cannot be made much thinner than several hundred nanometers due to the low absorption coefficient of the dye material. Furthermore, fabrication of each of the three organic dye filters for a red/green/blue or cyan/magenta/yellow color scheme requires carefully aligned lithography of each type of color filter over the entire photodiode array, thus making impractical the fabrication multicolor imaging devices with both large array formats and very small pixels.

On the other hand, the transmission properties of plasmonic metal filters composed of periodic hole arrays are mainly defined by their physical structure. This means that by simply changing the hole size, shape, and separation, the transmission spectra of the hole array can easily be controlled with only a single thin metal layer. Owing to this feature, plasmonic color filters are very cost competitive, especially for multicolor imaging applications. Furthermore, plasmonic filters have many other advantages over conventional filters, such as higher reliability under high temperature, humidity, and long-term UV radiation exposure conditions.

More recently, a plasmonic hole array color filter was integrated with a CMOS image sensor, demonstrating filtering functionality in the visible.[11,12] However, works such as this, have mostly focused on the transmission properties of large size filters with little emphasis given to other important filter performance aspects necessary for state-of-the art image sensor applications, such as the filter transmission dependence on array size, spatial color-crosstalk, and robustness against defects. In this work, we report on such optical properties as they pertain to various configurations of hexagonal arrays of

Received: June 5, 2012

   dx.doi.org/10.1021/nl302110z | *Nano Lett.* XXXX, XXX, XXX−XXX

subwavelength holes fabricated in 150 nm thick Al films suitable for image sensor integration.

In our experiments, hole array filter fabrication was done using a 30 kV, 10 pA focused ion beam (FIB) to mill the desired hole array patterns in a 150 nm thick Al film evaporated over 1 in. square quartz substrates. In order to characterize hole array transmission as a function of hole diameter and period in the visible wavelength range, we fabricated isolated square filters composed of 16 × 16 hexagonally aligned holes with period (p) ranging from 220 to 500 nm in 40 nm steps and diameter (d) ranging from 80 to 280 nm in 20 nm steps (see Figure 1).

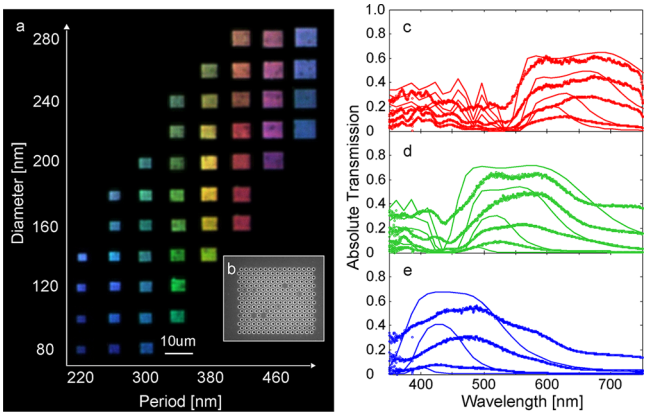

Figure 1. (a) Back illuminated microscope images of the fabricated hole array filters. Each filter consists of 16 × 16 hexagonally packed hole arrays. The vertical axis corresponds to hole diameter, ranging from 80to 280 nm in 20 nm steps, and the horizontal axis corresponds to hole period, ranging from 220 to 500 nm in 40 nm steps. The white bar on the lower part of the images corresponds to a 10 μm scale. Inset (b) shows a SEM image of a representative hole array filter consists of hexagonally aligned 16 × 16 holes with p = 420 nm and d = 240 nm. Measured hole array spectra for filters optimized to transmit (c) red (p = 420 nm, d = 160−280 nm), (d) green (p = 340 nm, d = 120−240 nm), and (e) blue light (p = 260 nm, d = 100−180 nm) are plotted in dotted lines, and the simulated spectra are plotted in solid lines. Each plot of three color spectra is in steps of 40 nm in hole diameter.

To analyze the transmission dependence on filter size, we designed filters that were optimized to operate at the three primary colors of (R) red (p = 420 nm, d = 240 nm), (G) green (p = 340 nm, d = 180 nm), and (B) blue (p = 260 nm, d = 140 nm) and fabricated four different hole array filter sizes of each corresponding to 1.2 × 1.2 μm^2, 2.4 × 2.4 μm^2, 5 × 5 μm^2, and 10 × 10 μm^2 size filters. To measure the effect of spatial color crosstalk between different color filters, we fabricated adjacent color filters adjoined with zero separation, and to determine the effect of random defects we fabricated 10 × 10 μm^2 size green filters with a density intentionally designed random defects ranging in area fraction from 1 to 50%.

Open windows with no metal film with the same physical aperture as the square hole array filters were fabricated in order to normalize filter absolute transmission efficiency. After milling the desired hole array configurations, the sample was covered with 200 nm of spin-coated Honeywell 312B spin-on-glass (SOG).

Spectral transmission measurements were performed on a Zeiss Axio Observer inverted microscope coupled to a grating spectrometer and nitrogen-cooled CCD system. The sample was illuminated with a halogen lamp filtered by a temperature conversion filter that gave a sunlike blackbody emission (color temperature of 5500 K) incident light. The microscope field diaphragm and aperture stop were both closed in order to have collimated incident light. All filter spectra were measured with a spectrometer utilizing a 100 × 1340 pixel liquid nitrogen cooled CCD detector with sensitivity in the 300−800 nm wavelength range. The transmission spectrum of each hole array filter was divided by the spectrum of the corresponding size open window in order to measure the absolute transmission of each filter. To check measurement system stability during characterization, the open window spectra were measured every hour.

Figure 1a shows a back-illuminated microscope image of the fabricated hole array filters consisting of arrays of 16 × 16 holes for each with hole period ranging from 220 to 500 nm from left to right and hole diameter ranging from 80 to 280 nm from bottom to top. The smallest 200 nm period filters correspond to ∼3.5 μm × 3.0 μm size filters, and the largest 500 nm period filters to ∼8.0 μm × 6.9 μm. The inset image (Figure 1b) shows a scanning electron micrograph (SEM) image of a representative filter with p = 420 nm and d = 240 nm.

The measured transmission spectra for the hole array periodicities corresponding to red (p = 420 nm), green (p = 340 nm), and blue (p = 260 nm) are plotted in Figure 1c,d, respectively, with each panel illustrating the spectra for different diameters. From the measured spectra, indicated as the color dotted lines, we see that the peak transmission position shifts to longer wavelength with increasing hole period and that the peak transmission efficiency increases with increasing hole diameter. The maximum filter transmission is found to be in the range of 40−50% in the visible spectrum with a spectral full-width half-maximum (fwhm) of ∼150 nm.

To validate the measured spectra, we simulated the fabricated filter transmission response using three-dimensional full-field electromagnetic simulations. The simulation model consists of a SiO_2 matrix with an embedded 150 nm thick Al film perforated with hexagonally aligned holes of the same pitch and diameter as those fabricated. The optical response of the resulting hole array film is excited with a broadband planewave source in the 300−900 nm wavelength range launched at normal incidence. The red solid lines in Figure 1c,d plot the resulting simulated transmission spectra. In general, the simulated profiles show good agreement with the measured spectra with the only notable differences being that the measured spectra have relatively broader profiles, which can be attributed to fabrication imperfections (e.g., tapered hole profiles) or surface roughness of the Al film.

Although the fabricated color filters reveal vivid colors and have fairly good peak transmission efficiency over the visible spectrum, there is some undesirable transmission in the blue spectral range for the red color filter designs. As evident from Figure 1, the red color filters (p = 420−500 nm, $d \geq$ 200 nm), optimized for transmission in the 600−800 nm wavelength range, demonstrate some spectral crosstalk with the blue part of the spectrum (λ_0 < 500 nm wavelengths). Owing to this undesirable transmission, the red color filters appear slightly pink, magenta, and violet as illustrated in Figure 1a. It is worth noting that although having perfect RGB filters would be most ideal for imaging applications, spectral crosstalk such as this can easily be corrected using signal processing.

Nevertheless, to better understand the origin of the spectral crosstalk, we used full-field simulations to spectrally resolved electric field distribution along the diameter of the holes, parallel to the polarization of the incident planewave. Figure 2

dx.doi.org/10.1021/nl302110z | Nano Lett. XXXX, XXX, XXX−XXX

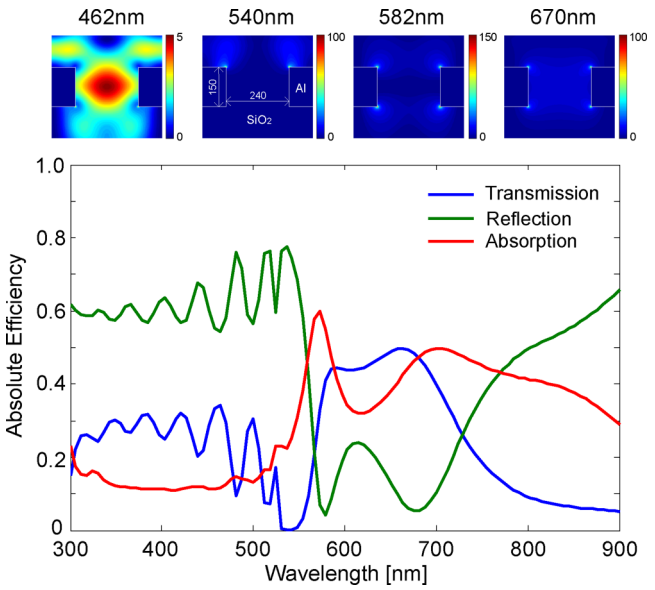

Figure 2. The simulated spectra of the hole array filter with p = 420 nm and d = 240 nm, which optimized to transmit red color. The top four panels plot the electric field distribution at the wavelengths of interest along the diameter of the holes, parallel to the polarization of the plane wave used to excite the structure.

shows the simulated transmission profile of the red (R) filter along with the cross-sectional electric field distributions at various wavelengths of interest. Consistent with our measurements, the simulated spectrum shows two broad transmission bands separated by a null at 540 nm that corresponds to the reciprocal lattice vector of the hexagonally aligned hole array structure.[6]

From the electric field intensity maps, we see that the transmission peaks at 582 and 670 nm of the longer wavelength transmission band correspond to strongly localized electric field distributions at the top and bottom of the hole, whereas for the transmission null at 540 nm, the localized electric field exists only at the top of the hole. This is consistent with the interpretation that there is an intrinsic $\pi/2$ phase shift resulting from the SPP emission and recapture process at the exit side of the film, leading to a minimum in the transmission at wavelengths corresponding to the reciprocal lattice vector of the array.[6]

On the other hand, whereas the electric field distribution at 582 and 670 nm show strongly localized field distributions at the top and bottom of the holes, the field distribution at 462 nm shows a high electric field intensity distribution inside the hole itself, suggesting that the source of transmission at shorter wavelengths is dominated by the photonic modes supported by the structure. We note that one way to reduce the excess blue transmission for the red filters may be to suppress these photonic modes via the use of coaxial structures rather than holes, formed by adding concentric metallic cylinders inside the hole. However the absolute transmission efficiency of coaxial structures has been reported to be only a few percent.[13,14]

Next, we investigate the effect of filter size on the transmission properties of hole array filters, an important feature in determining the smallest pixel size that can be used for imaging applications. The heavy lines in Figure 3 indicate the transmission spectra of the three primary color (RGB) hole array filters fabricated at four different filter sizes corresponding to squares of side-lengths equal to approximately 10 μm (Figure 3a), 5 μm (Figure 3b), 2.4 μm (Figure 3c), and 1.2 μm (Figure 3d). It is interesting to note that regardless of size, all the filters maintain their filtering functionality down to the 1 μm-size filters, although a cost in transmission efficiency. Both the 10 μm and 5 μm size filters have similar peak transmission efficiencies with blue peaking at 28% and green and red both at 38%. Transmission drops by ~25% for the 2.4 μm size filters relative to 10 μm size filters and by ~40% for the 1.2 μm size filters.

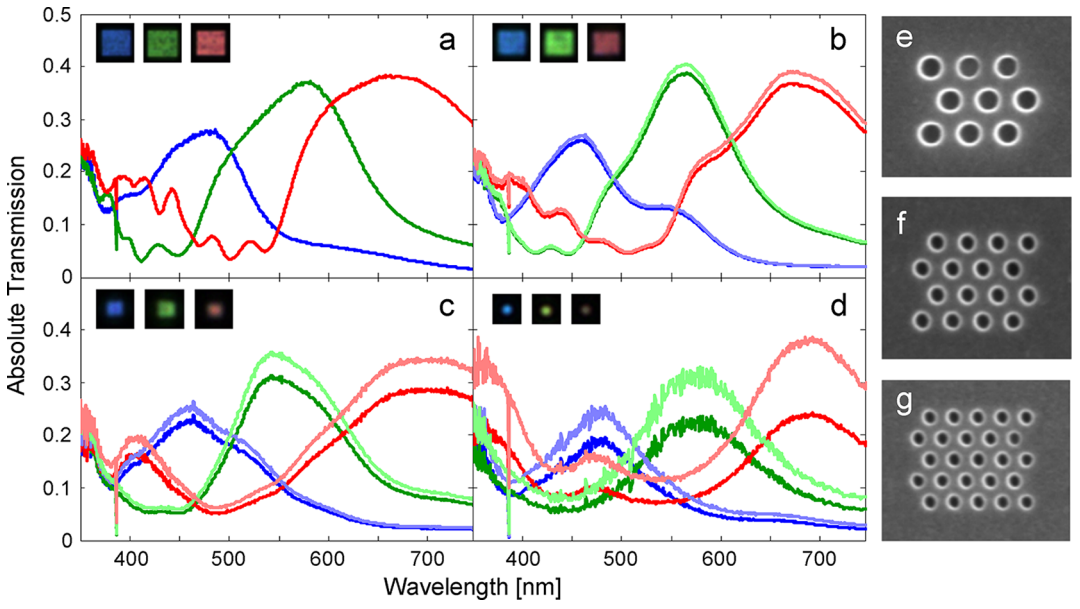

Figure 3. Transmission spectra of the hole array filters optimized to red (p = 420 nm, d = 240 nm), green (p = 340 nm, d = 180 nm), and blue (p = 260 nm, d = 140 nm) of different filter sizes of (a) 10 μm-, (b) 5 μm-, (c) 2.4 μm-, and (d) 1.2 μm-squared size filters. The insets of a-d panels show the back illuminated microscope images of the filter with the field of views corresponding to 13 μm-, 6.5 μm-, 5.0 μm-, and 4.0 μm-squared. (e)-(f) SEM images are the 1.2 μm-size filters, RGB, respectively.

dx.doi.org/10.1021/nl302110z | Nano Lett. XXXX, XXX, XXX–XXX

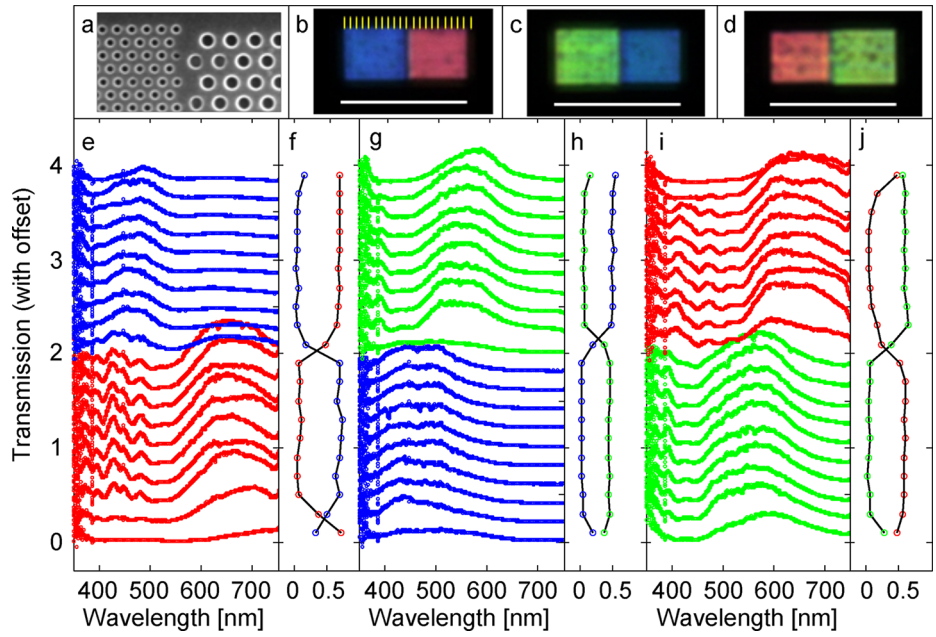

Figure 4. Sliced transmission spectra of color filter pairs with zero separation. (a) A representative SEM image of boundary between two such filters. (b–d) Back-illuminated microscope images of the color filter pairs taken with a color CCD camera. The white lines correspond to 20 μm scale bars. The spectra of each color filter pair are taken over 1 μm wide areas centered at the positions indicated by the yellow ticks in (b). Sliced spectra are shown for (e) blue/red, (g) green/blue, and (i) red/green filter pairs. The panels next to the sliced spectra in (f), (h), and (j) plot the correlation of each measured spectra with respect to the averaged spectrum of colors in the filter pair.

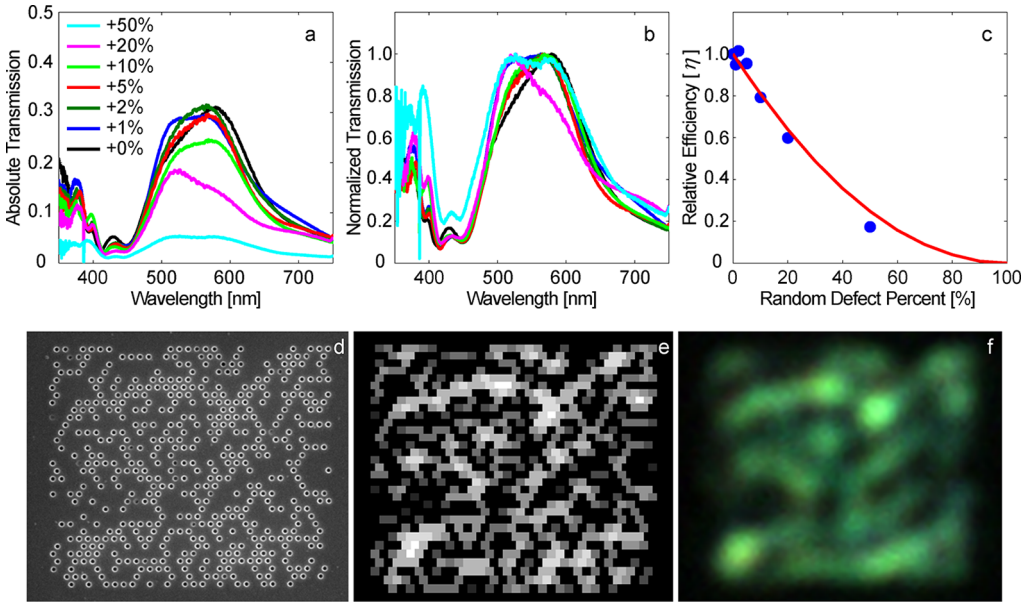

Figure 5. (a) Transmission spectra of green hole array filter consisting of 32 × 32 holes with p = 340 nm and d = 180 nm for different random defect (missing hole) density. (b) Normalized transmission spectra from (a). (c) Plot of the relative peak efficiency versus defect rate. The data plotted by blue dots corresponds to the transmission efficiency of a green filter with defect density ranging from 0 to 50% and the red line is the analytically estimated degradation curve. (d) A SEM image of green filter with 50% defect density. (e) An analytically calculated transmission intensity map of the filter from (d). (f) A back-illuminated microscope image corresponding to the filter from (d).

To investigate the effects of spatial crosstalk of colors between adjacent pixels, we measure the spectra of three different sets of color filter pairs with zero separation, consisting of B/R, G/B, and R/G color combinations, with each color filter consisting of a 10 × 10 μm^2 array. Figure 4a shows a representative SEM image of the boundary between two such hole array filters and Figure 4b–d show back illuminated images of the filter pairs. Figure 4e illustrates the measured sliced spectra for the B/R-filter combination with each spectrum corresponding to a 1 μm wide integrated cross-sectional area taken perpendicular to the filter pair boundary at the positions indicated by the yellow ticks in Figure 4b. Figure 4g,i shows the corresponding spectra for the other two filter pair color combinations.

The panel next to each sliced spectra, for example, Figure 4f, plots the correlation function Δ_i, which measures the difference

dx.doi.org/10.1021/nl302110z | Nano Lett. XXXX, XXX, XXX–XXX

between the measured spectrum, $T_i(\lambda)$, where i runs from 1 to 20 over the slice number, and the averaged spectrum of each filter color $\overline{T}_{R,G,B}(\lambda)$, obtained by averaging the middle eight spectra of each color filter. The correlation function is then defined by

$$\Delta_i = \alpha_i \int_{\lambda_{min}=400nm}^{\lambda_{max}=700nm} (T_i(\lambda) - \overline{T}_{R,G,B}(\lambda))d\lambda \quad (1)$$

where α_i is a normalizing constant for each measured spectrum, allowing Δ_i to take on values from 0 to 1 depending on the correlation of the measured spectra with respect to the averaged spectrum. In Figure 4f,h,j, the correlation functions undergo an inversion in going from one color filter to another. From these plots, we can estimate that the spatial color crosstalk between filters is as small as 1 μm. This length contains not only the contribution of the diffraction limit but also some defocus from the measurement settings, and hence it is possible that the crosstalk between filters is almost comparable to our detection limit. It is worth pointing out that although there is zero separation between the filters, Figure 4b−d clearly show dark lines between filter pairs, evidence of the small spatial color crosstalk between filters.

Because fabrication imperfections are inevitable, it is important to characterize the sensitivity of filter transmission and spectral shape to random defects. To evaluate the robustness of the hole array filter design, we measured the transmission of 32 × 32-hole green filters with randomly positioned missing holes at a density of 0, 1, 2, 5, 10, 20, and 50%. The resulting spectra are indicated in Figure 5a from which we can see that the filter transmission efficiency and shape is unaffected for random defect densities $\leq$5%, but filter transmission monotonically decreases for random defect densities $\geq$10%. However if we normalize each spectrum by its peak transmission as shown in Figure 5b, we find that all the spectra have the nearly identical line shapes, independent of filter defect density, suggesting that the random defects only affect the filter transmission efficiency and not the spectral shape.

To better understand the transmission efficiency degradation with increased defect density, we show the relative peak transmission efficiency versus random defect density in Figure 5c from which it is clear that the dependence is not simply linear, indicating that it is not simply a geometrical effect. To gain insight into the optical processes that govern this trend, we introduce a simple analytic model explain hole array transmission efficiency based on nearest neighbor interactions.

Because the hole array layout is three-fold symmetric, the filter transmission efficiency should not depend of the polarization of the incident light.[10] Thus, any given hole in the array, characterized by coordinates $x = i, y = j$, will have six equally distanced and thus equally contributing nearest neighbor sites, labeled A−F. Using this model, the transmission efficiency $\eta_{i,j}$ of each site in the array can be calculated by simply averaging the contribution from its nearest neighbors, as given by

$$\eta_{i,j} = \frac{1}{6}\sum_{k=A}^{F} \delta_k \quad (2)$$

where δ_k represents delta functions which will take on its value only if there is a hole at the nearest neighbor site, k. Using this model, the transmission efficiency of a given hole in the array will vary from 0 to 1, depending on the number of holes surrounding it. The relative transmission efficiency of a given filter, η, can then be calculated by summing over the efficiency of each hole in the array and normalizing it by the efficiency of a defect free array of the same size, $\eta_0 = 6($ number of holes in array$)$

$$\eta = \frac{\sum_{i,j\in array} \eta_{i,j}}{6(\text{number of holes in array})} \quad (3)$$

To check the accuracy of the model, we plot the predicted relative transmission efficiency of a 32 × 32 hole green filter as a function of random defect density in Figure 5c. From the correlation between the measured data and predicted curve, we see that the nearest-neighbor model correctly captures the degradation in efficiency with increasing number in random defects, suggesting that nearest neighbors indeed play the most dominant role is the transmission efficiency of hole arrays.

This nearest neighbor transmission model can also be used to reconstruct the spatial transmission distribution of a hole array filter with random defects. Figure 5d shows a SEM image corresponding to 32 × 32 hole green filter with 50% random defects. To predict the spatial transmission efficiency of this filter, we take the SEM image and apply the nearest neighbor transmission model to each site in the array. The resulting modeled transmission images are plotted in Figure 5e, which shows good qualitative agreement with the measured back illuminated image of the filter, Figure 5f.

Using this model, we can also explain the effect of filter size on the transmission properties of finite size defect-free hole array filters. For example, for a 3 × 3 filter, corresponding SEM image shown in Figure 3e, owing to the limited number of holes in the filter, only the center hole has six nearest neighbors and thus the maximum transmission. The other eight holes at the filter edge will have less than six neighbors, bringing down the average of the entire filter to 60%, as given by eq 2. However, for larger >24 × 24 hole filters, the transmission efficiencies go up to >95% because almost all the holes in the array have six nearest neighbors.

Using these relative transmission efficiencies, we can calculate the size-corrected transmission efficiency between two size filters of the same color by simply dividing their relative transmission efficiencies. To check this, we calculate and plot the size-corrected transmission profiles of the measured finite-size filters in Figure 3. The light lines in Figure 3b−d show the size-corrected spectrum of the 5, 2.4, and 1.2 μm size filters as compared to the 10 μm size filter. After the correction, we see that all four filters have fairly constant transmission efficiency, suggesting the model is also accurate in explaining finite size effects.

In conclusion, plasmonic hole array color filters are found to be a great alternative to conventional on-chip dielectric filters due to their tunability across the visible spectrum with only a single layer of perforated metal, especially for multicolor imaging applications. In this work, we show that because their scattering dynamics is only determined by nearest neighbor interactions, the transmission properties of hole array filters is extremely robust with respect to array size, random defects, and spatial crosstalk from neighboring filters of different color. The hole array's ability to filter light with only a small number of holes combined with their small spatial crosstalk are attractive features for 2D image sensor applications requiring densely packed filtering elements. Furthermore, their robustness filtering functionality against random defects make them

dx.doi.org/10.1021/nl302110z | Nano Lett. XXXX, XXX, XXX−XXX

especially tractable for industrial mass-production. However, for further developments of plasmonic filter technology to industrial application, additional studies, especially an actual filter implementation to a CMOS image sensor, are required to demonstrate their feasibility, reliability, and advantages to conventional technologies.

AUTHOR INFORMATION

Corresponding Author

*E-mail: haa@caltech.edu, sozo@caltech.edu.

Author Contributions

§Equal author contribution.

Notes

The authors declare no competing financial interest.

ACKNOWLEDGMENTS

This work was supported by the Air Force Office of Scientific Research under a Multidisciplinary University Research Initiative Grant FA9550-10-1-0264 and under Grant FA9550-09-1-0673. The authors gratefully acknowledge critical support and infrastructure provided by the Kavli Nanoscience Institute at Caltech. S.P.B. appreciatively acknowledges support from the National Science Foundation Graduate Fellowship.

REFERENCES

(1) Ebbesen, T. W.; Lezec, H. J.; Ghaemi, H. F.; Thio, T.; Wolff, P. A. Extraordinary optical transmission through sub-wavelength hole arrays. *Nature* **1998**, *391*, 667−669.

(2) Ghaemi, H. F.; Thio, T.; Grupp, D. E.; Ebbesen, T. W.; Lezec, H. J. Surface plasmons enhance optical transmission through subwavelength holes. *Phys. Rev. B* **1998**, *58* (11), 6779−6782.

(3) Barnes, W. L.; Dereux, A.; Ebbesen, T. W. Surface plasmon subwavelength optics. *Nature* **2003**, *424*, 824−830.

(4) Barnes, W. L.; Murray, W. A.; Dintinger, J.; Devaux, E.; Ebbessen, T. W. Surface plasmon polaritons and their role in the enhanced transmission of light through periodic arrays of subwavelength holes in a metal film. *Phys. Rev. Lett.* **2004**, *92* (10), 107401.

(5) Lezec, H. J.; Thio, T. Diffracted evanescent wave model for enhanced and suppressed optical transmission through subwavelength hole arrays. *Opt. Express* **2004**, *12* (16), 3629 2004.

(6) Pacifici, D.; Lezec, H. J.; Sweatlock, L. A.; Walters, R. J.; Atwater, H. A. Universal optical transmission features in periodic and quasiperiodic hole arrays. *Opt. Express* **2008**, *16* (12), 9222.

(7) Parson, J.; Hendry, E.; Burrows, C. P.; Auguie, B.; Sambles, J. R.; Barnes, W. L. Localized surface-plasmon resonances in periodic nondiffracting metallic nanoparticle and nanohole arrays. *Phys. Rev. B* **2009**, *79*, 073412.

(8) Lee, H.-S.; Yoon, Y.-T.; Lee, S.-S.; Kim, S.-H.; Lee, K.-D. Color filter based on a subwavelength patterned metal grating. *Opt. Express* **2007**, *15* (23), 15457.

(9) Chen, Q.; Cumming, D. R. S. High transmission and low color cross-talk plasmonic color filters using triangular-lattice hole arrays in aluminum films. *Opt. Express* **2010**, *18* (13), 14056.

(10) Inoue, D.; Miura, A.; Nomura, T.; Fujikawa, H.; Sato, K.; Ikeda, N.; Tsuya, D.; Sugimoto, Y.; Koide, Y. Polarization independent visible color filter comprising an aluminum film with surface-plasmon enhanced transmission through a subwavelength array of holes. *Appl. Phys. Lett.* **2011**, *98*, 093113.

(11) Chen, Q.; Chitnis, D.; Walls, K.; Drysdale, T. D.; Collins, S.; Cumming, D. R. S. CMOS photodetectors integrated with plasmonic color filters. *IEEE Photonics Technol. Lett.* **2012**, *24*, 3.

(12) Chen, Q.; Das, D.; Chitnis, D.; Walls, K.; Drysdale, T. D.; Collins, S.; Cumming, D. R. S. A CMOS image sensor integrated with plasmonic colour filters. *Plasmonics* **2012**, DOI: DOI: 10.1007/s11468-012-9360-6.

(13) Burgos, S. P.; de Waele, R.; Polman, A.; Atwater, H. A. A single-layer wide-angle negative-index metamaterial at visible frequencies. *Nat. Mater.* **2010**, *9*, 407−412.

(14) Si, G.; Zhao, Y.; Teo, S.; Zhang, M.; Huang, T. J.; Danner, A. J.; Teng, J. Annular aperture array based color filter. *Appl. Phys. Lett.* **2011**, *99*, 033105.